Magneto-Thermal Modeling of Second-Generation HTS for Resistive Fault Current Limiter Design Purposes

François Roy, *Student Member, IEEE*, Bertrand Dutoit, Francesco Grilli, and Frédéric Sirois, *Senior Member, IEEE*

***Abstract*—Coated conductors (CCs) are very promising for the design of novel and efficient resistive fault current limiters (FCLs). However, a detailed knowledge about their thermal and electromagnetic behaviors in the presence of over-critical currents is crucial for their improvement. In this context, we performed finite-element magneto-thermal modeling of CCs under over-critical current on several geometries. Accordingly, we have investigated the influence of the physical properties of stabilizer and substrate on the thermal stability to improve the high-temperature superconductor (HTS)-FCL design. All simulations were performed using COMSOL Multiphysics, a commercial finite-element package, which has a built-in coupling between the thermal and electrical equations, allowing us to compute both quantities simultaneously during the solving process. Our results allow us to determine the current threshold to achieve thermal stability of HTS FCLs made with CCs.**

***Index Terms*—COMSOL Multiphysics, fault current limiters (FCLs), finite-element methods (FEMs), high-temperature superconductors (HTS), thin-film devices.**

I. Introduction

RECENT advances in thin-film technology and epitaxial growth allow the emergence of coated conductors (CCs) as a second generation of high-temperature superconductors (HTS), which, by their anticipated low price and high critical current density, seems to be the favored candidate for resistive fault current limiters (FCLs) [1]–[3].

The main principle of HTS-FCL is to utilize the transition from the superconducting to the normal-conducting state by exceeding the critical current density of the superconductor. This transition is obtained by a succession of quench, i.e., an abrupt and localized loss of superconductivity. Hence, the FCL performance is dependent on the quench propagation which switches the whole superconducting material to the normal state and then limits the current flow with the increase of resistivity. As a result of low thermal diffusivity and inadequate energy dissipation, a considerable heating of the superconductive film can occur within the FCL. In the worst case, the HTS could not retrieve its superconducting state after the fault. Under these circumstances, all the nominal current passes through a much resistive material and the device finally burns out by a fast Joule heating.

In the recent past, several authors have proposed numerical magneto-thermal models to describe the behavior of CC-FCL [4]–[6]. Such simulations are of great interest to design efficient limiters since they allow having a better understanding of these devices, which are hard to design in a way that thermal stability is ensured over all conditions of operation. Nonetheless, numerical models proposed in the literature are usually not suitable for quick and simple calculations. Indeed, implementing home developed code or using typical finite-element method (FEM) software is often time consuming and requires considerable resources.

In this paper, we present a new magneto-thermal model that is very easy to implement. By using a simple $\vec{\mathbf{H}}$ formulation in two dimensions, we developed a numerical approximation to model high aspect ratio (AR) geometries ,which are always difficult to implement in FEM. Our simulations were developed using a widely used commercial software, hence providing us an easy way to share engineering with academics and industries.

II. Theoretical Model

In this section, we briefly introduce our coupled model, which simulates the electrical and thermal behavior of a typical HTS-FCL, as well as an AR approximation that allows us to drastically reduce the time required to perform the simulations.

Our geometrical model is based on commercial CCs available from Theva [7]. The coated HTS tapes are made of four layers. A thick conductive substrate layer made of Hastelloy C276, which is usually electrically isolated from the HTS, a MgO buffer layer, a superconductive film made of DyBCO $(DyBa_2Cu_3O_7)$, and a silver stabilizer in electrical contact with the superconductor.

In order to simulate the CC-FCL behavior, we used a 2-D geometry (a conductor of infinite length) 20 times thicker than the real one. As depicted in Fig. 1, we defined a model with three subdomains. We intentionally omitted the buffer layer, which does not influence importantly the electromagnetic and thermal behavior of the tape, to reduce the computation time.

Manuscript received July 30, 2007; revised December 19, 2007. This work was supported in part by the Swiss National Science Foundation through the National Center of Competence in Research "Materials with Novel Electronic Properties-MaNEP", and in part by the U.S. DOE Office of Electricity Delivery and Energy Reliability. This paper was recommended by Associate Editor S. W. Schwenterly.

F. Roy and B. Dutoit are with École Polytechnique Fédérale de Lausanne, EPFL-IC-LANOS, 1015 Lausanne, Switzerland (e-mail: francois.roy@epfl.ch; bertrand.dutoit@epfl.ch).

F. Grilli was with the Los Alamos National Laboratory, Los Alamos, NM 87545 USA. He is now with École Polytechnique de Montréal, Montréal, QC, H3C 3A7, Canada (e-mail: f.grilli@polymtl.ca).

F. Sirois is with École Polytechnique de Montréal, Montréal, QC, H3C 3A7, Canada (e-mail: f.sirois@polymtl.ca).

Digital Object Identifier 10.1109/TASC.2008.917576

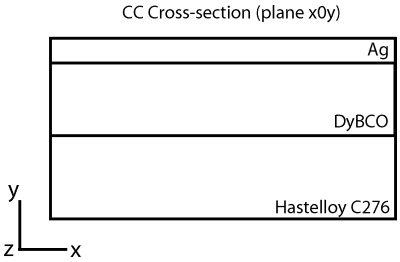

Fig. 1. Cross section of the simulated CC (not drawn to scale). The tape is 10 mm wide and is composed of three subdomains: 1) Hastelloy substrate, 2) DyBCO film, and 3) an Ag stabilizer. We intentionally omitted the MgO buffer layer to reduce the computation time of our simulations.

TABLE I
GEOMETRICAL PARAMETERS (20 TIMES THICKER)

Parameters	Expression (μm)	Description
t_{Ag}	59 to 120	Thickness of silver layer
t_{DyBCO}	60	Thickness of DyBCO layer
t_{Hast}	1800	Thickness of hastelloy layer
w	10000	Width of tape

TABLE II
ELECTRICAL PARAMETERS

Parameters	Expression	Description
E_0	1E-4 Vm^{-1}	Critical field
f	50 Hz	Frequency of imposed current
J_{c_0}	1E10 Am^{-2}	Critical current density at T_0 [7]
α	1.5	$J_c(T)$ law exponent [8]
ρ_{norm}	130E-8 Ωm	DyBCO resistivity at T_c [7]
ρ_{Ag}	1E-8 Ωm	Ag resistivity near T_0
ρ_{Hast}	120E-8 Ωm	Hastelloy resistivity

TABLE III
THERMAL PARAMETERS

Parameters	Expression	Description
T_0	77 K	Boiling temperature of LN2
T_c	90 K	Critical temperature of DyBCO
k_{Ag}	429 $\mathrm{W(mK)}^{-1}$	Heat conductivity of Ag [9]
Cp_{Ag}	235 $\mathrm{J(kgK)}^{-1}$	Heat capacity of Ag [9]
ρ_{m-Ag}	10500 kgm^{-3}	Ag mass density [9]
k_{SC}	7 $\mathrm{W(mK)}^{-1}$	Heat conductivity of DyBCO [7]
Cp_{SC}	180 $\mathrm{J(kgK)}^{-1}$	Heat capacity of DyBCO
ρ_{m-SC}	9000 kgm^{-3}	DyBCO mass density [7]
k_{Sap}	1000 $\mathrm{W(mK)}^{-1}$	Heat conductivity of sapphire
Cp_{Sap}	60 $\mathrm{J(kgK)}^{-1}$	Heat capacity of sapphire
ρ_{m-Sap}	3990 kgm^{-3}	Sapphire mass density
k_{Hast}	7 $\mathrm{W(mK)}^{-1}$	Heat conductivity of Hastelloy
Cp_{Hast}	425 $\mathrm{J(kgK)}^{-1}$	Heat capacity of Hastelloy
ρ_{m-Hast}	8940 kgm^{-3}	Hastelloy mass density

The complete set of parameters used for our simulations is listed in Tables I, II, and III.

The magneto-thermal model was implemented in COMSOL Multiphysics [10], an FEM open structure software that allows great freedom to deal with partial differential equations. One of the main advantages of COMSOL is the built-in simultaneous coupling of the thermal and electrical systems of equations. This way to proceed is more convenient than coupling electromagnetic and thermal solvers, which requires a frequent exchange of information between the two solvers, with a consequent increase of the computation time.

A. Electrical Model

The electromagnetic model is based on the work of Brambilla *et al.* [11] on the development of an edge-element model for ac loss computation of HTS. The formulation, briefly summarized here, is based on a direct use of the magnetic field $\vec{\mathbf{H}}$ as a state variable.

From Faraday's law, the coupling of the magnetic and electric fields is described as

$$\nabla \times \vec{\mathbf{E}} = -\frac{\partial \vec{\mathbf{B}}}{\partial t} \tag{1}$$

where $\vec{\mathbf{E}} = E_z$ is the longitudinal electric field given by the nonlinear relation

$$E_z = \rho(J_z) J_z \tag{2}$$

the current density is obtained by the Ampère's Law, which in quasi-static 2-D approximation is expressed as

$$J_z = \frac{\partial H_y}{\partial x} - \frac{\partial H_x}{\partial y}. \tag{3}$$

In order to simplify the notation, we will omit the z subscript for J_z and E_z in the remainder of the paper.

The input parameter, i.e., the transport current in our case, is imposed by the boundary conditions that the integral of the magnetic field on the border of a circular domain, representing the liquid nitrogen (LN2), equals the source current at each time step

$$I_{src}(t) = \oint \vec{\mathbf{H}} dl'. \tag{4}$$

The use of edge elements guarantees the continuity of the tangential component of the magnetic field from one element to the adjacent one. In this way, the equation $\nabla \cdot \vec{\mathbf{B}} = 0$ does not have to be added to the model, since it is automatically satisfied [12].

As explained in [11], this formulation has numerous advantages over usual potential formulations, namely avoiding the choice of a gauge and the postdifferentiation of the electromagnetic potentials, which may introduce inaccuracies in the solution variables. However, the major drawback of the $\vec{\mathbf{H}}$ formulation is related to the difficulty to model a voltage source.

Indeed, no potential term naturally appears in the $\vec{\mathbf{H}}$ formulation. Although it would be important to eventually take into account voltage sources and coupling with other circuit elements, such as the electrical load of the circuit, this is not a critical issue for demonstrating the validity of the magneto-thermal formulation proposed here.

The macroscopic behavior of the HTS is described by means of a nonlinear resistivity, which depends, in our model, on the temperature and local current density (see Fig. 2). In the absence of experimental data, we used a combined exponent power law to illustrate our ability to introduce complex nonlinear functions

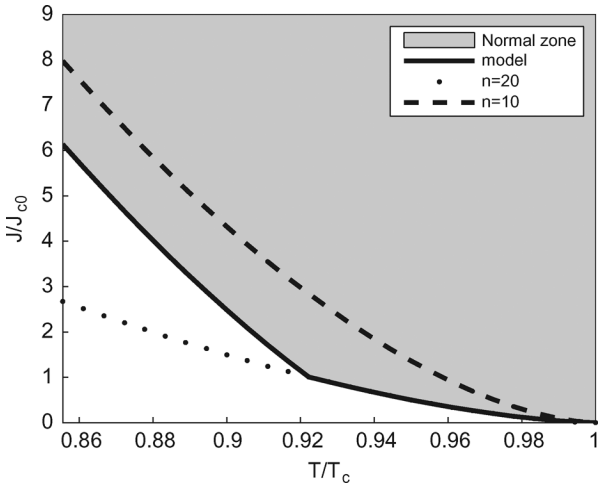

Fig. 2. Normal resistivity frontier as a function of J and T. Our model is a combination of two power laws, i.e., $n = 10$ and $n = 20$. The shaded area at the right of the curve represent the normal state (i.e., $\rho = 130E - 8\Omega.\text{m}$).

in our model. For the purpose of this paper, we used $n = 20$ for $J < J_c$ and $n = 10$ for $J \geq J_c$

$$\rho(J,T) = \begin{cases} \rho_{pl}(J,T), & T < T_c \\ \rho_n, & T \geq T_c | \rho_{pl}(J,T) \geq \rho_n \end{cases} \quad (5)$$

$$\rho_{pl}(J,T) = \frac{E_0}{J_c(T)} \left(\frac{|J|}{J_c(T)} \right)^{n-1} \quad (6)$$

$$n = \begin{cases} 20, & J < J_c \\ 10, & J \geq J_c \end{cases} \quad (7)$$

$$J_c(T) = J_{c_0} \left(\frac{T_c - T}{T_c - T_0} \right)^{\alpha}, \quad T < T_c. \quad (8)$$

B. Thermal Model

A local increase of temperature in the HTS results in a reduction of the critical current which, in turn, changes the curl of the magnetic field and the electric field inside the tape. This field generation is responsible for a heat dissipation through the HTS that induces the loss of the superconducting state and may, ultimately, destroy the FCL. To avoid that, heat generated by the Joule effect must be evacuated efficiently by means of conduction as well as thermal exchange with liquid nitrogen. This last mechanism, called pool boiling, is largely responsible of the heat transfer and usually ensures the thermal stability of the device during its operation.

Generally speaking, pool boiling is dependent on the tape surface temperature (see Fig. 3). When the surface temperature T_s is close to the boiling temperature of the fluid T_0, heat transfer is mostly governed by free convection (region a). A further increase of temperature (region b) causes the apparition of vapor bubbles that nucleate on the CC surface. Due to the latent heat, large thermal exchange occurs in this range of temperature. However, when the vapor covers more areas on the heated surface, a considerable degradation of the heat transfer is observed due to the fact that thermal conductivity of the vapor is much less than that of the liquid (region c). At large temperature differences, the solid-liquid interface becomes notably weak and a vapor film completely covers the heated surface. In this final

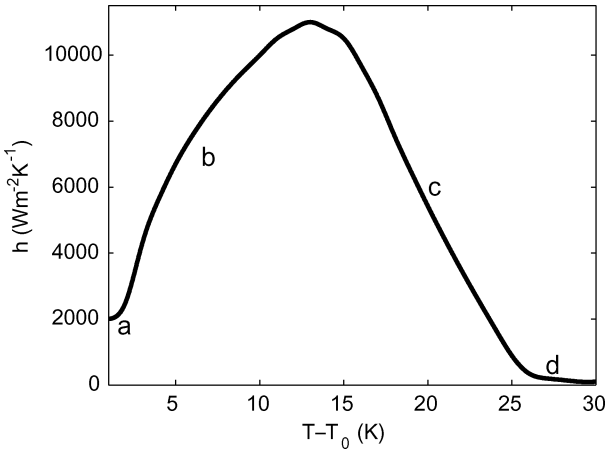

Fig. 3. Convective heat transfer coefficient for the model [13]. (a) free convection; (b) nucleate boiling; (c) transition boiling; and (d) film boiling.

stage (region d), the heat transfer is very low and the tape becomes almost thermally isolated from its surroundings.

Our thermal model is based on a transient conduction equation, which is expressed as

$$Q = \rho_m C_p \frac{\partial T}{\partial t} - \nabla \cdot (-k \nabla T) = E_Z \cdot J_z \quad (9)$$

where Q is the power density dissipated in the tape, ρ_m is the subdomain mass density, C_p the heat capacity, and k the thermal conductivity tensor.

In order, to take into account the pool boiling, we used a "convective" heat flux at the interface between the tape and LN2. The strongly temperature-dependent cooling power of LN2 is thus replaced by an equivalent thin pseudo-heat-conduction layer

$$\hat{\mathbf{n}} \cdot (k_i \nabla T) = h(T_s - T_0) \quad (10)$$

where h is termed the convection heat transfer coefficient and i is the subdomain in contact with LN2.

This simplified approach to simulate pool boiling at the coolant boundary is very powerful in many situations, especially if the main interest is not the flow's behavior but rather its cooling power.

C. Numerical Approximations

The simulations were developed in 2-D for lower AR than the real FCL shape. This is on account of the difficulty of meshing geometries of high AR that usually involves a large number of deformed elements. Following the work of Duron *et al.* [14], four physical parameters have been scaled in the thicker geometry to approximate the real solution. These parameters are C_p, J_{c0}, k, and E.

Succinctly, the adopted numerical scheme is as follows. In all our simulations, we kept the real total current in the hypertrophied tape, which is Γ time thicker than the real one. To do so, we divide J_{c0} by this Γ factor for the lower AR geometry. We also multiplied E by this factor to take into account the tape cross section (which is Γ times larger). For the thermal set of equations, the increase of the y dimension has been implemented by a multiplication of k_y by Γ. A division of C_p by the Γ factor was also set to be consistent with the mass gain of

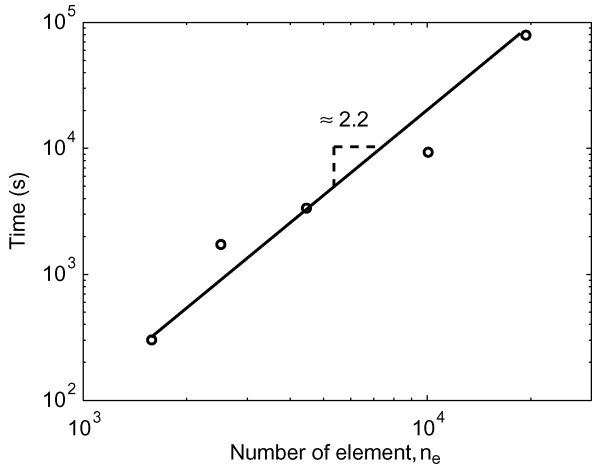

Fig. 4. Computation time as a function of the number of element (n_e). The dashed lines represent the slope of the curve.

the tape. Finally, we divide k_x by Γ, whereby to preserve the thermal diffusivity on the x direction.

In order to validate our approximations, we have quantitatively compared the impact of different tape AR on the state variables of our electrical and thermal models, i.e., H_x, H_y, and T. Obviously, as the AR decreases (thicker tape), our approach introduces important inaccuracies on the magnetic field profile at the tape extremities. Fortunately, the relative error observed on the associated temperature profiles was negligible (less than 0.1%).

Using lower AR geometries allows us to reduce the number of elements required to keep the convergence and accuracy of our model: with a reduced number of nodes, the shape of the elements and, consequently, the quality of the interpolated results can be improved. Fig. 4 illustrates the influence of the problem size on the computation time. From this figure, we can observe that the calculation time increases roughly as $\approx (n_e)^{2.2}$. These times are obtained on a dual Xeon quadcore E5355 with a 2.66-GHz clock speed and 8GB of RAM memory. In our case using an AR 20 times larger allows reducing the number of elements from 19346 to 2516, which corresponds to a reduction of the computation time by 45.

III. Numerical Results

In this section, we investigate the influence of the imposed current on the HTS stability threshold. In addition, the effect of electrical connectivity between the tape layers as well as the stabilizer thickness and substrate materials are computed on the HTS-FCL behavior near the current threshold. We also look at the thermal parameters' impact on the thermal diffusivity and corresponding tape temperature response.

As discussed previously, due to our formalism, we used a typical fault current waveform instead of a real short-circuit (see Fig. 5). The nominal current amplitude is 267 A, corresponding to 89% of the critical current of the tape. The peak of the current faults is 800.36 A during less than 5 ms.

Also, we depicted in Fig. 5 the mean electric field associated to this current waveform, integrated on the tape cross-section. Although not the same as the voltage we would measure

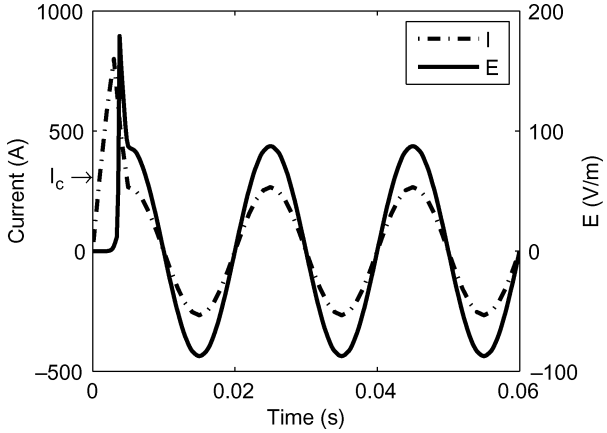

Fig. 5. Fault current waveform of the source and associated cross section mean electric field for a typical simulation ($I_{\rm peak} = 800.36$ A).

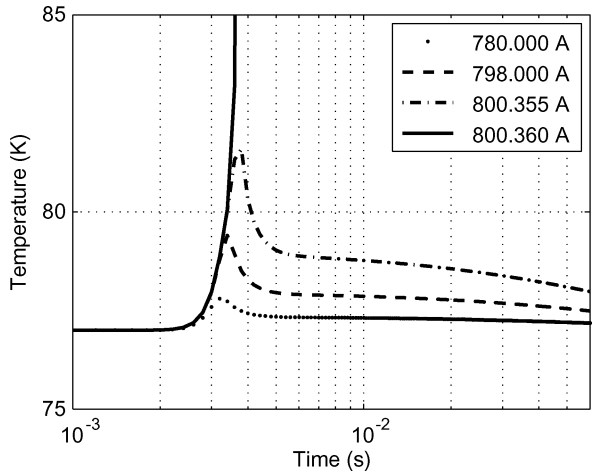

Fig. 6. Effect of the current on the thermal stability. The threshold current is around 800 A for this model. The temperature is quite constant within the HTS layer, hence we took the temperature at the center of the HTS film.

across device terminals, it indicates that a magneto-thermal steady-state condition is reached almost instantaneously within the sample.

A. Peak Current Threshold

Using a coated superconductor allows us to attain higher critical current density than massive conductors. Nevertheless, the small thickness of CCs makes them very sensitive to temperature excursions.

As depicted in Fig. 6, a very small fluctuation of the imposed current (less than 5 mA) is responsible for a sudden warming of the device. This is due to the high thermal inertia of the tape, which avoids the rapid cooling of the conductor and the recovery of the superconducting state. Under these circumstances, a current threshold is established for which the thermal stability is lost.

B. Impact of a Shunted Tape

Therefore, the rapid recovery seems impossible once the HTS has switched to his normal state. This is particularly true if the tape does not have a shunt resistance (i.e., Ag and/or hastelloy) to absorb a part of the dissipated energy. This is what we can

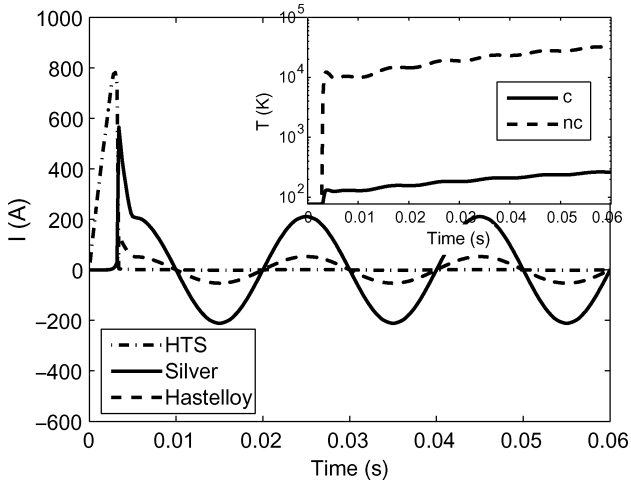

Fig. 7. Distribution of the current ($I_{\rm peak} = 810$ A) in the subdomains for a shunted tape (substrate and stabilizer). The inset is the temperature of the tape for a shunted (c) and nonshunted (nc) device. For a nonshunted configuration, all the current goes in the HTS which has a high resistivity in the normal state. This has a direct effect on the temperature increase.

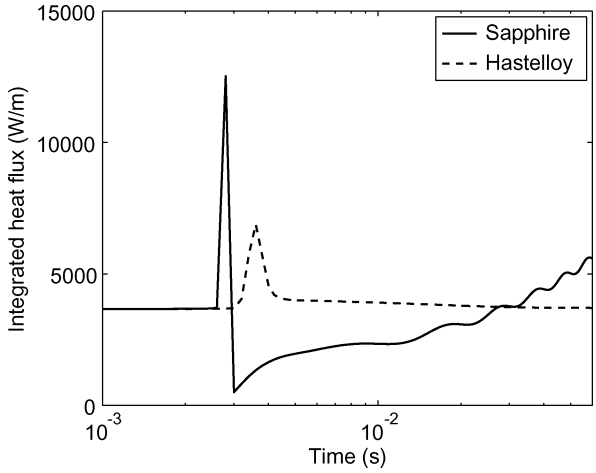

Fig. 9. Integrated heat flux, which is defined as $\oint h(T_s - T_0)dl$, represent the heat exchange between the tape and the coolant. The surface temperature of the sapphire substrate increases rapidly and makes suddenly the convective coefficient reaching the film boiling region (the observed drop). At this stage, the tape is almost "isolated" from the coolant and it burns out quickly. $I_{\rm peak} = 800.355$ A.

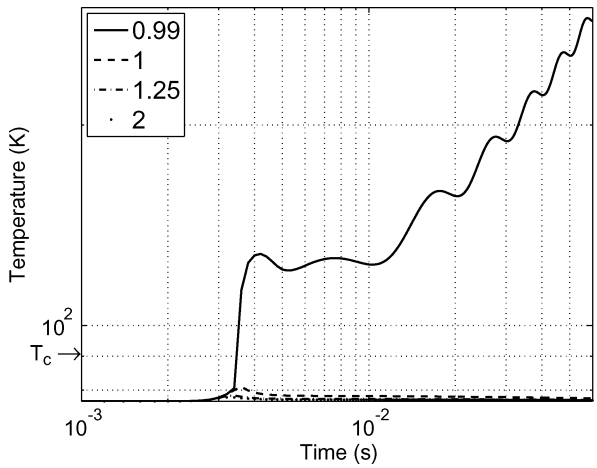

Fig. 8. Effect of the Ag/HTS thickness ratio on the temperature for a three-cycle simulation. The temperature is quite constant within the HTS layer, hence, we took the temperature at the center of the HTS film. $I_{\rm peak} = 800.36$ A.

observe in Fig. 7. The normal resistance of the HTS, which is higher than that of the substrate and stabilizer (we do not introduce a temperature dependence for the resistivity of these layers), makes the power generated within the DyBCO practically negligible in comparison to that in the silver film. In this case, the superconducting state will be recovered only if the stabilizer film succeeds in trading the generated heat with the nitrogen bath before the next current peak is reached.

C. Influence of the Stabilizer Thickness

Since silver is a better conductor than hastelloy (see Table II), it is interesting to study the influence of the stabilizer thickness on the heat dissipation. The Ag/HTS thickness ratio, to be thermally stable, depends on $I_{\rm peak}$. However, as displayed in Fig. 8, an increase of the silver thickness (relatively to the HTS thickness) can favor the thermal stability by acting as a buffer zone to absorb heat and reduce the current density responsible of the heat generation within the stabilizer.

In spite of the positive effects on thermal stability, using a thicker stabilizer has a side effect on the limitation capability of the device. As a matter of fact, if there is an electrical contact between the HTS film and a conducting layer, the layer shunts the film in the normal state, and a part of the current flows through the other electrically connected part of the tape, as simple parallel resistors. Adding a parallel resistance lowers the global resistance of the tape, so that more current can flow in the tape without attenuation. This leads to a decrease of losses in the HTS film and, on the other hand, produces Joule losses in the conductive parallel paths. Accordingly, the shunted limiter requires more tape length to limit the same imposed current.

D. Effect of the Substrate Material

The materials constituting the tape have an important influence on the thermal exchange between the coolant and the tape surface. As depicted in Fig. 9, by comparing two usual CC substrates, such as hastelloy and sapphire, we observe that a rapid increase of the surface temperature induces a huge drop on the thermal flux within the tape-coolant interface. The combination of a low heat capacity and a high thermal conductivity gives sapphire a thermal diffusivity (defined as $\alpha_d = k/\rho_m C_p$) that is more than 1000 times larger than hastelloy. However, the heat, which is not readily stored in the sapphire substrate, cannot be released due to a kind of bottleneck effect.

Fig. 10 allows us to observe the stability criteria for these two cases (i.e., hastelloy and sapphire substrate). Stability recovery occurs when the heat removed to the substrate and coolant ($Q_{\rm out}$) is greater than that generated within the superconductor ($Q_{\rm in}$). The dotted line plotted in Fig. 10 is the graphical illustration of this criteria which is defined as

$$\frac{Q_{\rm in}}{Q_{\rm out}} = \frac{\left[\int_A \vec{\mathbf{E}}.\vec{\mathbf{J}}dA'\right]_{\rm HTS} + \left[\int_A \vec{\mathbf{E}}.\vec{\mathbf{J}}dA'\right]_{Ag}}{\oint h(T_s - T_0)dl}. \qquad (11)$$

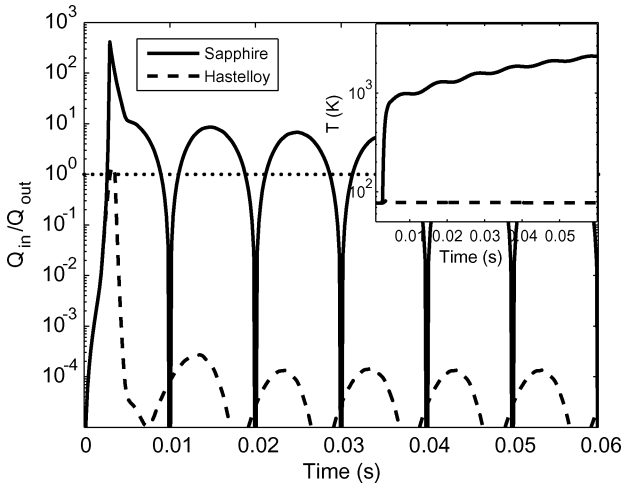

Fig. 10. Comparison of the heat balance for different substrate material. The heat generated in the tape made of sapphire is not evacuated at all. The temperature is continuously increasing until the device burned out. Inset is the temperature for both samples. $I_{\rm peak} = 800.355$ A.

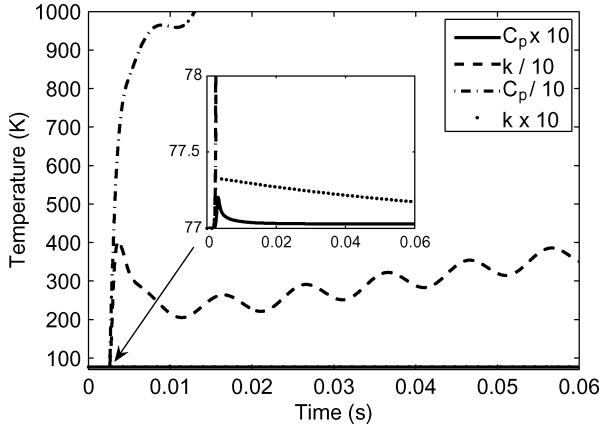

Fig. 11. Impact of the heat diffusivity on the temperature profile. By multiplying k by 10 or by dividing C_p by 10, we obtain a thermal diffusivity 10 times larger than the one used in Fig. 6 for $I_{\rm peak} = 800.355$ A. On the other hand, by dividing k by 10 or multiplying C_p by 10 we reduce the thermal diffusivity by a factor of 10. We observe that an increase of the heat capacity has a positive effect on the thermal stability.

We can see that the sample made of sapphire has a notable energy gain at each half-cycle which also produces the continuous increase of the temperature (see the inset of the Fig. 10). For this particular case, we can observe that the tape burned out almost instantaneously at the first current peak.

The hastelloy curve let us observe that the denominator of (11), which is the LN2 exchange term, rapidly gets higher than the heat generation term (numerator). This leads to a fast thermal equilibrium with the surrounding coolant. Moreover, we observe in this figure that a "phase shift" exists between the produced energy within the hastelloy-made tape and the imposed current to the device. This comes from the flux diffusion phenomenon in the superconducting state, in which losses continue to occur within the sample through magnetic relaxation even if the source current is zero. In the case with the sapphire, the temperature gets so high that superconductivity is rapidly lost, therefore no relaxation process exists.

E. Effect of the Heat Capacity

Finally, we observe that an increase of the thermal diffusivity is not a synonym of success to attain readily the thermal stability. Indeed, Fig. 11, shows that the key factor is the heat capacity instead of the thermal conductivity. In this figure, we investigate the influence of the thermal parameters C_p and k on the temperature profile of a tape submitted to a threshold current of 800.355 A. Strangely, even if an increase of the heat capacity reduces the thermal diffusivity, we observe that an increase of the heat capacity has a positive effect on the thermal stability. This is in accordance with our previous guess concerning the stored energy in the hastelloy substrate.

IV. Conclusion

In this paper, we have presented a new finite-element model for studying electromagnetic and thermal behavior of HTS, specifically for FCL applications. The model, coupling the electromagnetic and thermal equations in a single solving process, is simpler to implement and much faster than other models based on solving the two parts separately and exchanging the results at each time step. The model, having been implemented in a widely used commercial software package (both in academic and industrial environment), provides an easy way to share engineering knowledge between users. It is ready to be tested against experimental data and to be used to design FCL applications. In addition, it is open to a number of possible improvements:

1) Introduce the temperature dependence of physical parameters such as the heat capacity and the thermal conductivity.
2) Introduce the field dependence of the critical current density of the superconductor (as previously done by Hong *et al.* [15]).
3) Extend the model to 3-D (see Pecher *et al.* [16]).
4) Optimize the solving process by testing different mesh element types, tolerances, solvers, etc.
5) Couple voltage sources and classical circuit elements to the magneto-thermal model.

References

[1] W. Prusseit, G. Sigl, R. Nemetschek, C. Hoffmann, J. Handke, A. Lümkemann, and H. Kinder, "Commercial coated conductor for fabrication based on inclinated substrate deposition," presented at the ASC 2004, Jacksonville, FL, Oct. 4–8, 2004, Paper 1MR07.

[2] Y. Li, J. Reeves, X. Xiong, Y. Qiao, Y. Xie, P. Hou, A. Knoll, K. Lenseth, and V. Selvamanickam, "Fast growth process of long-length YBCO coated conductor with high critical current density," *IEEE Trans. Appl. Supercond.*, vol. 15, no. 2, pp. 2771–2774, Jun. 2005.

[3] M. C. Ahn, D. K. Bae, S. E. Yang, D. K. Park, T. K. Ko, C. Lee, B. Y. Seok, and H. M. Chang, "Manufacture and test of small-scale superconducting fault current limiter by using the bifilar winding of coated conductor," *IEEE Trans. Appl. Supercond.*, vol. 16, no. 2, pp. 646–649, Jun. 2006.

[4] M. Lindmayer and H. Mosebach, "Quenching of high-Tc-superconductors and curent limitation—Numerical simulations and experiments," *IEEE Trans. Appl. Supercond.*, vol. 7, no. 2, pp. 1029–1032, Jun. 1997.

[5] T. Rettelbach and G. J. Schmitz, "3D simulation of temperature, electric field and current density evolution in superconducting components," *Supercond. Sci. Technol.*, vol. 16, pp. 645–653, 2003.

[6] J. Duron, F. Grilli, L. Antognazza, M. Decroux, B. Dutoit, and Ø. Fischer, "Finite-element modelling of YBCO fault current limiter with temperature dependent parameters," *Supercond. Sci. Technol.*, vol. 20, no. 4, pp. 338–344, 2007.
[7] Theva 2007 [Online]. Available: www.theva.com
[8] S. R. Curràs, J. Viña, M. Ruibal, M. Gonzàlez, M. R. Osorio, J. Maza, J. A. Veira, and F. Vidal, "Normal-state resistivity versus critical current in $YBa_2Cu_3O_{7-\delta}$ thin films at high current densities," *Physica C*, vol. 372–376, pp. 1095–1098, 2002.
[9] D. R. Lide, Ed., *CRC Handbook of Chemistry and Physics*, 87th ed. Boca Raton, FL: CRC Press, 2006–2007.
[10] COMSOL 2007 [Online]. Available: www.comsol.com
[11] R. Brambilla, F. Grilli, and L. Martini, "Development of an edge-element model for AC loss computation of high-temperature superconductors," *Supercond. Sci. Technol.*, vol. 20, pp. 16–24, 2007.
[12] J. P. Webb, "Edge elements and what they can do for you," *IEEE Trans. Magn.*, vol. 29, no. 2, pp. 1460–1465, Mar. 1993.
[13] W. Frost and W. L. Harper, *Heat Transfer at Low Temperatures*. New York: Plenum, 1975, ch. 4.
[14] J. Duron, L. Antognazza, M. Decroux, F. Grilli, S. Stavrev, B. Dutoit, and Ø. Fischer, "3-D finite element simulations of strip lines in a YBCO/Au fault current limiter," *IEEE Trans. Appl. Supercond.*, vol. 15, no. 2, pp. 1998–2002, Jun. 2005.
[15] Z. Hong, A. M. Campbell, and T. A. Coombs, "Numerical solution of critical state in superconductivity by finite element software," *Supercond. Sci. Technol.*, vol. 19, pp. 1246–1252, 2006.
[16] R. Pecher, M. D. McCulloch, S. J. Chapman, L. Prigozhin, and C. M. Elliot, "3D-modelling of bulk type-II superconductors using unconstrained H-formulation," presented at the EUCAS 2003, Sorrento, Italy, Sep. 14–18, 2003.

François Roy (S'06) received the B.Eng. degree in physical engineering from Université Laval, Québec, QC, Canada, in 2004. In 2006, he received the M.Sc. degree in energy and material sciences from the Institut National de la Recherche Scientifique (INRS-EMT), Varennes, QC, Canada, where he worked on the copper surface modification by plasma-based ion implantation for the improvement of arc systems cathodes. He is now with École Polytechnique Fédérale de Lausanne, Switzerland, as a Ph.D Student where he is currently working on the modeling and characterization of resistive second-generation HTS fault current limiters.

Bertrand Dutoit received the M.S. degree in physics from the University of Lausanne, Switzerland, his Certificates in environmental protection and management from the Swiss Federal Institute of Technology, Lausanne, Switzerland, and from the Swiss Graduate School of Public Administration, Lausanne, Switzerland, and the Ph.D. degree from the University of Lausanne, in 1983, 1986, 1988, and 1992, respectively. His Ph.D. dissertation was entitled "Magneto-Optical Study of the Intermediate State in Type-I Superconductors."

Currently, he is a Project Leader and Head of the Superconductivity Group, Laboratory of Nonlinear Systems, École Polytechnique Féedérale, Lausanne, Switzerland. He is also teaching applied superconductivity. His research interests include nonlinear modeling and superconductivity with a focus on the measurements and characterization techniques of high-temperature superconductors.

Francesco Grilli received the M.S. degree in physics from the University of Genoa, Italy, in 1998, and the Ph.D. degree from the Swiss Federal Institute of Technology-Lausanne, Switzerland, in 2004. His Ph.D. dissertation was entitled "Numerical Modeling of High Temperature Superconducting Tapes and Cables."

From October 1999 to August 2000, he was a Software Engineer with Marconi Communications, Genoa, Italy. From September 2000 to July 2004, he was a Teaching and Research Assistant at the Laboratory of Nonlinear Systems of the Swiss Federal Institute of Technology-Lausanne. From August 2004 to August 2007, he was a Postdoctoral Research Associate at the Superconductivity Technology Center of the Los Alamos National Laboratory, Los Alamos, NM. He is currently a postdoctoral fellow at École Polytechnique de Montréal, Montréal, QC, Canada. His main research interests are the 2-D and 3-D modeling of high-T_c superconductors and devices and the dc and ac characterization of their properties.

Frédéric Sirois (S'96–M'05–SM'07) received the B.Eng. degree in electrical engineering from Université de Sherbrooke, Sherbrooke, QC, Canada, in 1997, and the Ph.D. degree from École Polytechnique de Montréal, Montréal, QC, Canada, in 2003. From 1998 to 2002, he was affiliated as a Ph.D. scholar with Hydro-Québec's Research Institute (IREQ).

From 2003 to 2005, he was a Research Engineer at IREQ. In 2005, he joined École Polytechnique de Montréal as an Assistant Professor. His main research interests include modeling of electromagnetic and superconducting devices, integration of superconducting equipments in power systems, and planning of power systems.